

Superior Gas-Sensing Performance of Amorphous CdO Nanoflake Arrays Prepared at Room Temperature

Ye-Qing Zhang,^{a†} Zhe Li,^{a†} Tao Ling,^a Sergei A. Kulinich^{b,c,*}, and Xi-Wen Du^{a,†,*}

^a Key Laboratory of Advanced Ceramics and Machining Technology, Ministry of Education, Tianjin University, Tianjin 300072, P.R. China

^b Institute of Innovative Science and Technology, Tokai University, 4-1-1 Kitakaname, Hiratsuka, Kanagawa 259-1292, Japan

^c Aston Institute of Photonic Technologies, Aston University, Aston Triangle, Birmingham B4 7ET, United Kingdom

[†]The two authors contributed equally to this work

* Address correspondence to skulinich@tokai-u.jp; xwdu@tju.edu.cn

Abstract

Highly sensitive and selective detection of volatile organic compounds (VOCs) with fast response time is imperative based on safety requirements, yet often remaining a challenge. Herein, we propose an effective solution, preparing a novel gas sensor comprised of amorphous nanoflake arrays (a-NFAs) with specific surface groups. The sensor was produced via an extremely simple process in which a-NFAs of CdO were deposited directly onto interdigital electrode immersed in a chemical bath under ambient conditions. Upon exposure to a widely used VOC, diethyl ether (DEE), the sensor exhibits excellent performance, more specifically, the quickest response, lowest detection limit and highest selectivity ever reported for DEE as target gas. The superior gas-sensing properties of the prepared a-NFAs are found to arise from their open trumpet-shaped morphology, defect-rich amorphous nature, and surface C=O groups.

Keywords: gas sensor, VOC, nanoflake arrays, chemical bath deposition

Introduction

Many of volatile organic compounds (VOCs), which are common chemicals for industrial applications, are deemed as hazardous due to their flammability and toxicity. Therefore, development of gas sensors for monitoring such VOCs is imperative based on the safety requirements¹. Diethyl ether (DEE) is a widely used VOC which is well known for its anesthetic effect and a continued exposure to which may lead to respiratory failure or even death². Therefore, its highly-selective and quick detection is of high importance.

The materials commonly used for monitoring DEE are oxide semiconductors (e.g. CdO, SnO₂, and TiO₂) with three-dimensional (3D) architecture³⁻⁵. These materials demonstrate certain attractive features such as high sensitivity, good stability, and low working temperature. For instance, Fu et al. reported on the synthesis of a hierarchical CdO nanostructure with a novel bio-inspired morphology and an excellent response toward DEE³. Yu and coworkers prepared a NiO-modified TiO₂ porous film which exhibited a high sensitivity to DEE⁵. However, there is still much room for improving DEE detection. On one hand, the selectivity of so far developed sensors to DEE remains at a low level since they also exhibit similar response to other VOCs such as acetone, methanol, ethanol and so on^{1,6}. On the other hand, even the best reported response time is still quite long, being close to or over 10 s^{3,6,7}. Thus, the current sensors cannot meet the requirements for practical applications. In addition, the metal oxide nanostructures for the above mentioned sensors are fabricated at high temperatures, which makes the production of such devices rather complex and expensive⁸⁻¹⁰.

Recently, amorphous nanomaterials such as CuO, MoO₃, and TiO₂ have attracted extensive attention in the field of sensors as they are prepared at low temperatures and contain abundant defects which act as active sites for gas sensing¹¹⁻¹³. Various synthetic approaches, such as sol-gel, sputtering and pyrolysis, have been employed to fabricate such amorphous oxides¹⁴⁻²⁰. Compared to the above mentioned methods, the chemical bath deposition (CBD), known as a prevailing low-temperature approach for producing large-area thin films, exhibits certain advantages. It does not require any complex instruments and/or special substrates, and the precursors used are commonly available and inexpensive²¹.

Functional groups on the sensing material surface are known to play a crucial role in its gas-sensing properties, contributing via different mechanisms, such as, e.g., hydrogen bonding and polar interactions²²⁻²³. For instance, hydroxyl and carboxyl groups were reported to be beneficial for the adsorption of target gas by graphene oxide sensors²², while nitro groups were found to govern the response intensity of carbon-based sensors to ammonia²³. Therefore, gas-sensing materials with amorphous structure and controlled surface groups are greatly anticipated for highly-sensitive sensors with high selectivity and excellent performance.

In this work, we developed a simple one-step strategy to produce gas sensors that detect DEE quickly yet with high sensitivity and selectively. A simple and cost-efficient CBD approach was employed to produce amorphous nanoflake arrays (a-NFAs) of CdO with specific surface groups directly onto interdigital electrode at room temperature. Upon exposure to DEE, the as-prepared and then heat-treated

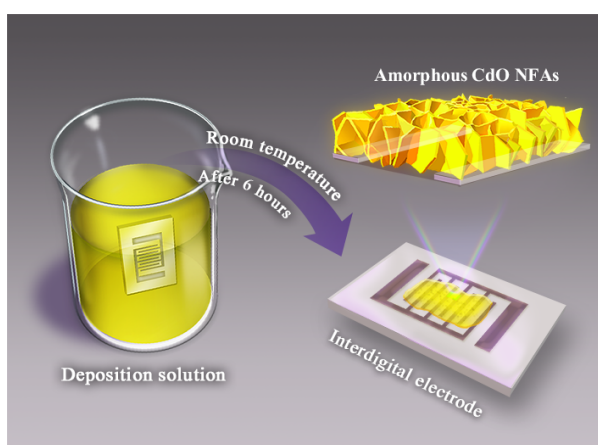
a-NFAs showed the quickest response (4.5 s), lowest detection limit (5 ppm) and highest selectivity (3.5) reported to date. The observed excellent performance was attributed to the unique structure of the a-NFAs, more specifically, their (i) open trumpet-shaped morphology, (ii) amorphous nature and (iii) specific surface groups. The open structure of the flakes allows for a quick infusion and adsorption of DEE, thus improving the response speed efficiently. The amorphous phase with a large number of surface defects can absorb gas molecules efficiently and facilitates a low detection limit, while the abundant surface groups (mainly C=O) attract specifically DEE rather than other VOCs, thus enhancing gas selectivity.

1. Experimental Section

Materials. All chemical reagents used, CdCl₂ (cadmium chloride, >99.0 %), thiourea ((NH)₂CS, >99.0 %), TEOA (tris(2-hydroxyethyl)amine, >98.0 %), and NH₃·H₂O (ammonium hydroxide, 0.1N standardized solution), were purchased from Alfa Aesar Co., Ltd. and used without further purification. Two types of substrates, glass coated with fluorine-doped SnO₂ (FTO) and commercial interdigital electrode form Beijing Elite Tech Co., Ltd, were chosen for the growth of a-NFAs via CBD and further sensor fabrication.

Synthesis of CdO a-NFAs. Scheme 1 presents the simple and inexpensive process used in this study to prepare a sensing layer of CdO NFAs. Commercial interdigital electrode, with 0.2-mm-wide gap between comb-shaped Ag-Pt contacts on ceramic, was used as substrate. Prior to deposition, the substrates were washed with a detergent solution in water, after which sonicated successively with acetone, deionized water

and ethanol. Finally, the cleaned interdigital electrode was dried with nitrogen gas. The aqueous solution used for the CBD contained a mixture of cadmium chloride (0.1 M) and thiourea (0.1 M). The total volume of the mixture was kept as 80 mL, to which TEOA (5 % by volume) was added as a complexing agent. Ammonium hydroxide was also added to keep the pH of the chemical bath at 11.5 ± 0.1 . The interdigital electrode was then immersed vertically into the bath for 6 h to form a-NFAs. The process was carried out at room temperature and relative humidity in the test chamber of 30%, thus being very simple and cost-efficient.



Scheme 1. Schematic illustration of preparation of a-NFAs via CBD on interdigitated electrode.

Physical Characterization. The morphology of samples was observed using scanning electron microscopy (SEM, Hitachi S-4800) at an acceleration voltage of 5 kV, and the composition was measured by an Oxford INCA energy-dispersive X-ray spectroscopy (EDS) module attached to the SEM instrument. Transmission electron microscopy (TEM) images, selected area electron diffraction (SAED) patterns and electron energy loss spectroscopy (EELS) spectra were obtained in a Technai G2 F20 TEM tool with an

acceleration voltage of 200 kV. The phase structure of the material was investigated with X-ray diffractometry (XRD, Bruker D8 advance). X-ray photoelectron spectroscopy (XPS) analysis was performed using a Kratos Axis Ultra spectrometer (with monochromated Al K α irradiation). A pass energy of 20 eV was used for narrow-scan spectra and 80 eV for survey scans. All spectra were calibrated by using C 1s peak (284.6 eV) as the reference. Atomic force microscopy (AFM, Agilent 5500) was applied to determine the thickness of the prepared CdO flakes. Surface groups were investigated with Fourier-transform infrared spectroscopy (FTIR, Bruker Tenser-27).

Gas Sensing Tests. Prior to gas-sensing tests, each NFA-based device was heat-treated at its test temperature (typically 175 °C) for 24 h to stabilize its morphology and chemical composition. The sensors were tested in a computer-controlled gas-detecting system (CGS-1TP, Beijing Elite Tech Co., Ltd), with humidity in the test chamber typically being 30%. A certain volume of liquid analytes (acetone, DEE, ethanol, or methanol) was injected with a microsyringe onto a glass-plate heater in the test chamber, and the concentration of the evaporated gas was calculated according to the total volume (18 L) of the chamber. Here, the response of the sensor was defined as the ratio $R_{\text{gas}}/R_{\text{air}}$ (for DEE) or $R_{\text{air}}/R_{\text{gas}}$ (for acetone, ethanol, or methanol), where R_{gas} and R_{air} are the electrical resistances of the sensor in the presence of test gas and in air at the same operation temperature, respectively. The response time is defined as the time required to reach 90% of the final response upon exposure to target gas.

3. Results and Discussion

The gradual growth of a CdO deposit resulting in NFAs is shown in Figure 1. A layer of

nanoparticles first nucleated and grew on the substrate, after which sparse nanoflakes emerged (Figures 1 a,b). As time elapsed, such separate nanoflakes grew larger both horizontally and vertically, eventually transforming into continuous NFAs well-seen in Figures 1c,d.

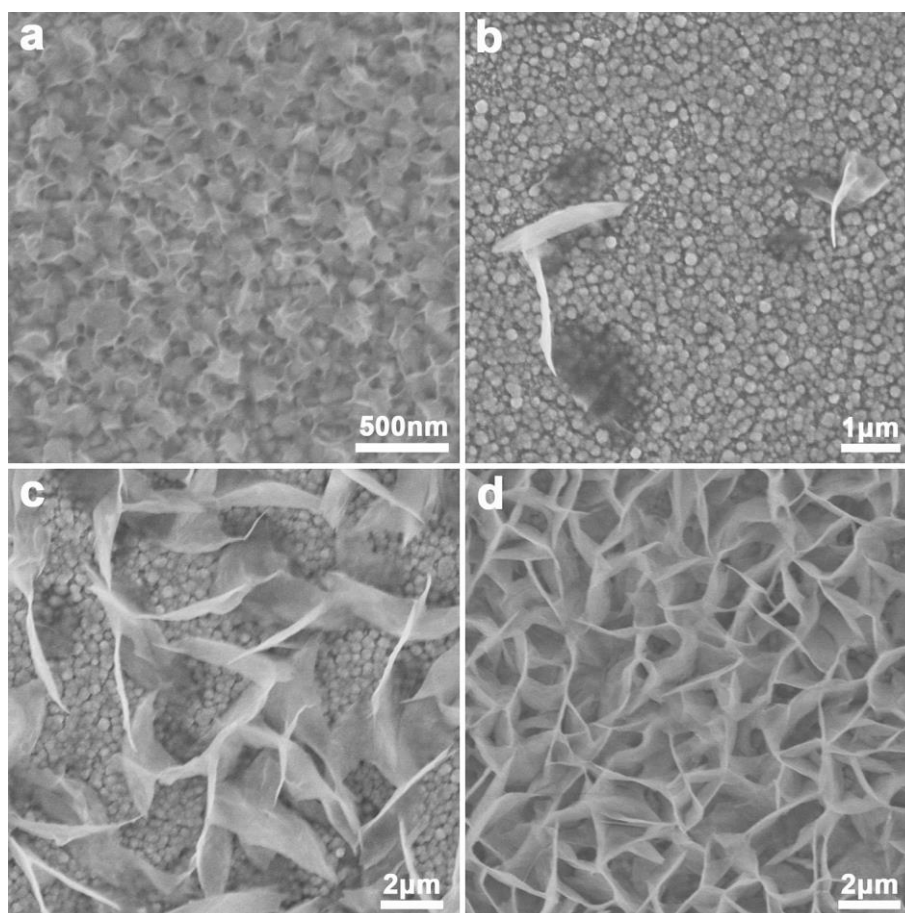


Figure 1. Morphology evolution of growing a-NFAs over time. SEM surface images of the sample after (a) 2.5, (b) 3.5, (c) 4.5, and (d) 5.5 h in chemical bath.

A top-down view SEM image in Figure 2a reveals that the as-prepared sample is composed of uniform NFAs with an average flake size of 700 nm. The inset in Figure 2a shows the cross-sectional SEM image of the product. The thickness of the NFA layer prepared on the electrode is about 1 μm and there is a thin layer under the NFAs, in agreement with Figure 1a. The HRTEM image and SAED pattern in Figure 2b suggest

an amorphous structure of the nanoflakes. AFM analysis indicates the thickness of a single nanoflake is around 9 nm (Figure 2c).

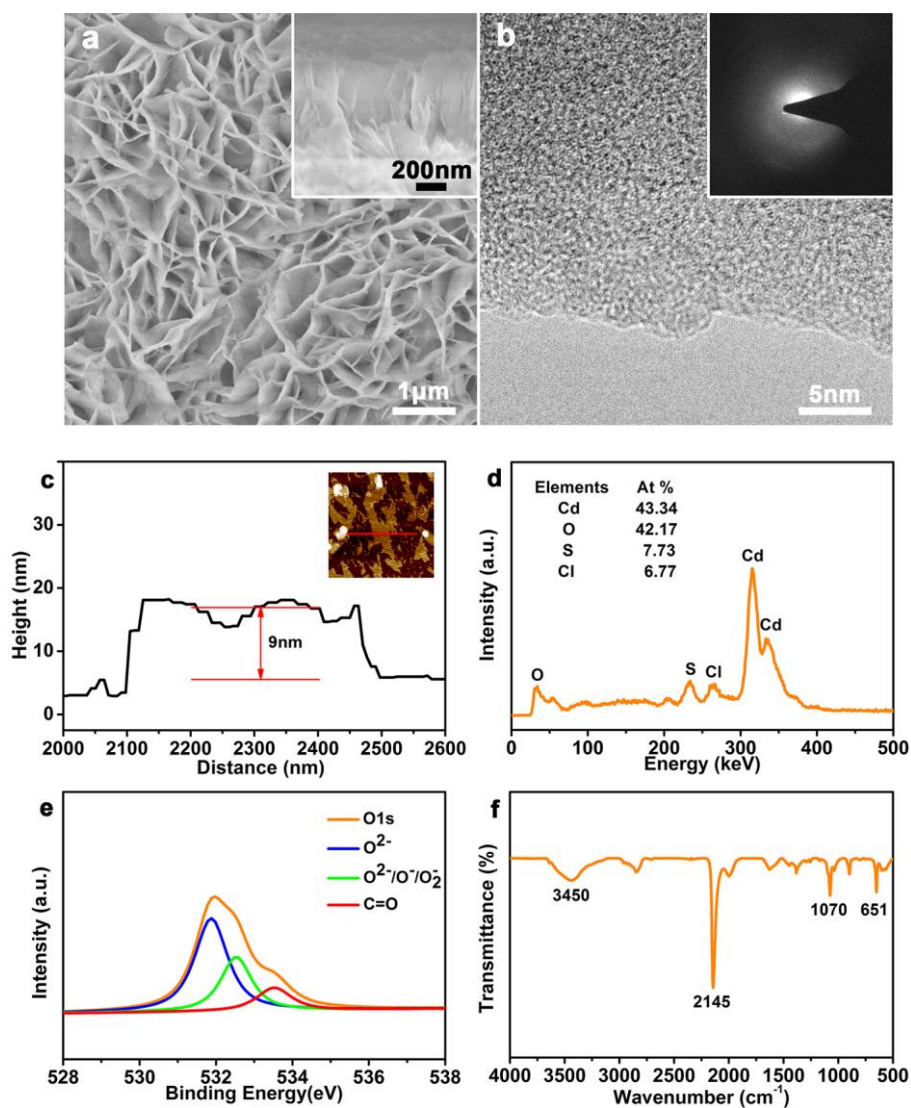


Figure 2. Characterization of prepared a-NFAs. (a) Top-view SEM image of as-prepared NFA layer, the inset is a cross-sectional SEM image with scale bar indicating 1 μm. (b) HRTEM image; the inset is an SAED pattern. (c) AFM profile of a single nanoflake lying flat on mica substrate. (d) EDS spectrum of as-prepared a-NFAs. (e) XPS O1s spectrum showing the binding energy of oxygen species. (f) FTIR spectrum of as-prepared CdO NFAs.

The composition and chemical bonding of the prepared a-NFAs were investigated by means of EDS, XPS, FTIR and EELS. The EDS spectrum in Figure 2d presents

signals of Cd, S, Cl and O, where sulfur and chlorine atoms come from thiourea and cadmium chloride, respectively. Quantitative EDS and XPS results reveal that the detected atomic ratio of cadmium to oxygen is close to one, suggesting the composition of the product CdO (see Figure S1). Meanwhile, the XPS Cd d3/2 peak consisted of two components located at 405.1 and 411.8 eV (Figure S2), both of which arise from Cd²⁺ species. The EELS profile of the sample displays two peaks at 534.84 and 404.23 eV, corresponding to the O²⁻ K-edge and Cd²⁺ M-edge absorption, respectively (Figure S3) and confirming the above mentioned CdO composition of the material.

XPS and FTIR spectra were analyzed to reveal the surface groups in the prepared a-NFAs. The XPS O1s spectrum in Figure 2e can be deconvoluted into three components at 531.87, 532.53 and 533.51 eV, which are assigned to “bulk” oxygen (O²⁻), adsorbed oxygen species (such as O²⁻, O⁻ and O₂⁻) and oxygen-containing functional groups (such as C=O), respectively²⁴. The FTIR spectrum in Figure 2f suggests the presence of surface C-O (1070 cm⁻¹), C=O (1633 and 2145 cm⁻¹) and Cd-O (651 cm⁻¹) bonds²⁵⁻²⁷. Particularly, the most intense peak appears at 2145 cm⁻¹, implying that the oxygen-containing surface groups are mainly C=O ones. The Mott-Schottky plot of the a-NFAs is presented in Figure S4, with a positive slope in its linear region confirming the n-type character of the a-NFAs.

The gas sensing performance was evaluated directly by measuring the electrical resistance of the flakes on interdigital electrode as seen in Figure 3a. The working temperature is known to have a remarkable influence on sensing response of gas sensors^{1,3}. As clearly seen in Figure S5, the electrical resistance of CBD-prepared a-NFAs increases upon exposure to 200

ppm of DEE. At a fixed working temperature, the sensor showed a stable on/off response upon several adsorption/desorption cycles (Figure S6). The optimal working temperature is seen in Figure S5 to be 175 °C. Therefore, all the subsequent measurements were carried out at this working temperature. The effect of humidity on sensor performance was also tested (Figure S7), the obtained results suggesting the sensor was not sensitive to atmospheric humidity and its response remained basically unchanged within the humidity range of 30 to 50 %.

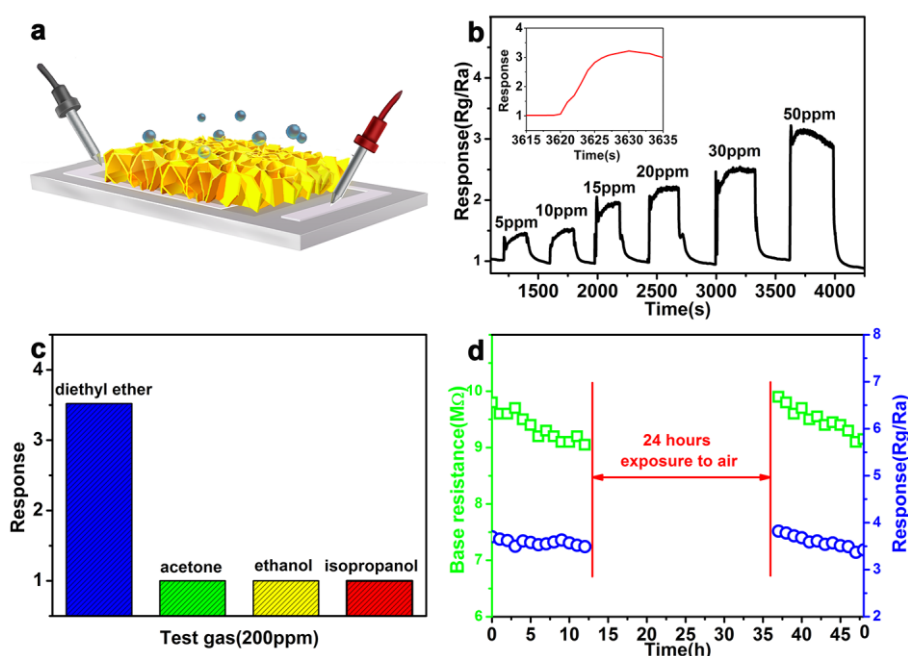


Figure 3. (a) Schematic illustration of gas-sensing device based on an interdigitated electrode coated with CdO NFAs. (b) Dynamic response curve of the sensor to DEE with concentrations ranging from 5 to 50 ppm recorded at 175 °C. The inset is an enlarged part of panel (b), illustrating the average response time of the sensor to be 4.5 s. (c) Response of the sensor based on a-NFAs to various VOCs with a concentration of 200 ppm at 175 °C. The sensor exhibits a particularly high selectivity and a considerable response to DEE. (d) Stability of working sensor over time. After working at 175 °C and 200 ppm of DEE for 12 h, the base resistance and response of the sensor slightly decrease, however they recover back to their initial level after exposure to air for 24 h.

Next, the detection limit of the sensor was tested. The device was found to respond well to

DEE even at concentrations as low as 5 ppm (Figure 3b), its response being 1.60 and 1.75 at 5 and 10 ppm of DEE, respectively, which is high enough for signal identification. Moreover, the response time to DEE was as short as 4.5 s (see the inset in Figure 3b), which is the fastest response to this VOC of all sensors reported in the literature (Table 1).

It is worth mentioning that the number of reports on DEE detection are quite limited, being mainly focused on 3D structures as such structures have large specific surface area, which is thought to be advantageous for gas adsorption and desorption. In addition, such sensors based on 3D structures are seen in Table 1 to have reasonably short response times. To stress out the importance of the trumpet-like 3D structure of the obtained NFAs for their gas sensing properties, we also tested a sensor based on similar amorphous CdO nanoparticles (Figure S8). In our experiments, when rough substrates were used, such nanoparticles were prepared via CBD instead of ANFs. The results presented in Figure S8 demonstrate that the response of the nanoparticle-based sensor was lower (2.8), while its response time was about 10 times longer (~50s).

Table 1. Comparison of different gas sensors for DEE detection

Sensing Material	Synthetic Temperature (°C)	Response Time (s)	Selectivity	Detection Limit (ppm)	Ref.
CdO a-NFAs	25	4.5	3.5	5	This work
Hierarchical CdO	170	8	1.35	50	[3]
Porous TiO ₂ film	500	400	3.5	10	[5]
Carbon nanotubes	1200	90-130	1.25	N/A	[6]

Selectivity to particular gases is another key property for practical applications of gas sensors. So far, no ideal gas sensor with good selectivity to DEE has been reported in the literature^{1,3,6}. Intriguingly, the NFA-based sensor fabricated in this study showed an excellent selectivity to DEE. As shown in Figure 3c and Figure S9, at 200 ppm, the sensor's response to other VOCs, including acetone, ethanol and isopropanol, is not noticeable, implying a good selectivity to DEE.

The stability and durability of the sensor working at 175 °C over a long period of time were also evaluated. As shown in Figure 3d, the device's response to 200 ppm of DEE slightly decreases from 3.5 to 3.3 after 12 h of non-stop testing. The NFAs in the sensor were found to retain their morphology and phase composition after the test (Figure S10), suggesting good stability of the CBD-prepared amorphous NFAs. Moreover, upon exposure of the sensor to air for 24 h, the device was found to regain its response back (Figure 3d). The decrease in the sensors' base resistance observed in Figure 3d is believed to be due to a gradual elimination of surface C=O groups during long-term heating at 175 °C. As a result, the material's ability to bound electrons somewhat drops and its base resistance decreases. However, when placed in air at room temperature, the nanoflake surface is gradually oxidized by O₂ and H₂O, thus regaining surface C=O groups and recovering its initial surface conductivity. Thus, the combination of a low detection limit for DEE, quick response, good selectivity, and high stability makes the CBD-prepared a-NFAs a very promising material for gas sensing (in particular for DEE sensing).

Finally, the sensor's long-term performance was evaluated. It was subjected to 30 cycles, each of which consisted of 8 h of non-stop run with 200 ppm of DEE at 175 °C and

16 h of exposure to air. The results are presented in Figure S11, where it is seen that the base resistance and response eventually decreased from 9.6 to 8.0 and from 3.5 to 3.2, respectively. Thus, after being tested under very harsh conditions for 240 h, the sensor demonstrates only a slight attenuation in its performance.

When compared with other gas-sensing materials, the CBD-prepared CdO NFAs possess an amorphous structure and surface groups which are believed to be responsible for their unique sensing properties, especially the excellent selectivity to DEE. To clarify the role of both the structure and surface groups, the material (deposited onto FTO glass) was annealed for 1 h in air at 275 and 350 °C. As shown in Figure 4a, the morphology of nanoflakes remained mainly unchanged even after annealing at 350 °C, while the surface roughness of each nanoflake increased. XRD results indicate that crystallization occurs during annealing at both 275 and 350 °C (Figure 4b). FTIR spectra demonstrate that the surface C=O groups were stable after long-term testing at 175 °C and annealing at 275 °C for 1 h, while their density (manifested by peaks at 1633 and 2145 cm^{-1}) was significantly reduced after annealing at 350 °C (see Figure 4c). Based on the above, the amorphous NFAs with abundant surface C=O groups completely transform into crystal phase after annealing at 275 °C and lose their surface groups after heat treatment at 350 °C. Correspondingly, as seen in top panel of Figure 4d and Figure S12, the gas sensor annealed at 275 °C remained highly selective to DEE, though its response (2.8) was somewhat lower than that of as-prepared a-NFAs (3.5). In contrast, the sensor annealed at 350 °C did not respond to DEE in the same way, while showing high response to ethanol and isopropanol (bottom panel in Figure 4d and Figure S13).

This implies that the sensor's selectivity to DEE originates from its surface C=O groups rather than the amorphous structure of nanoflakes.

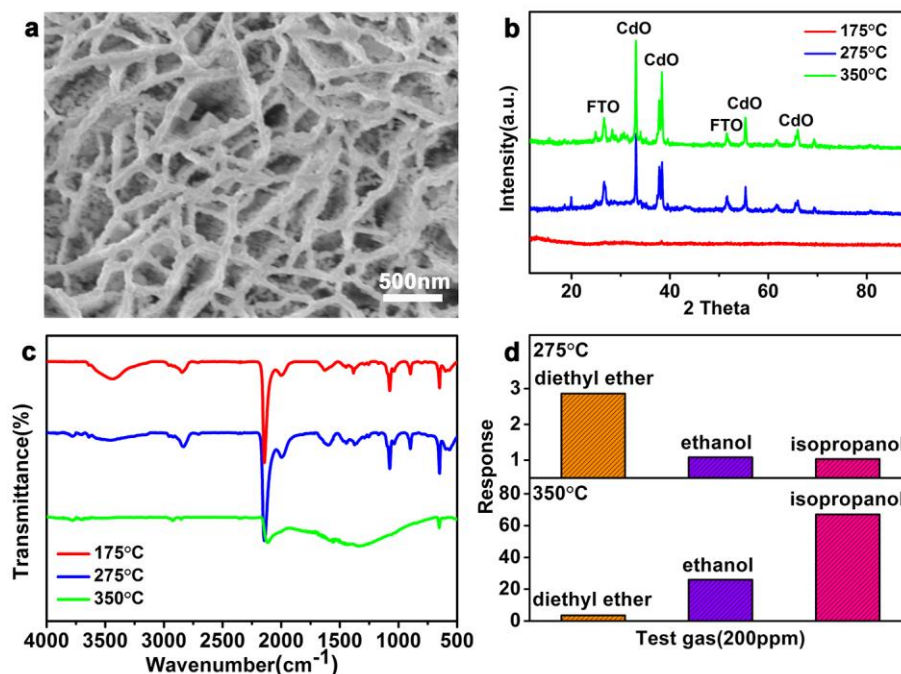
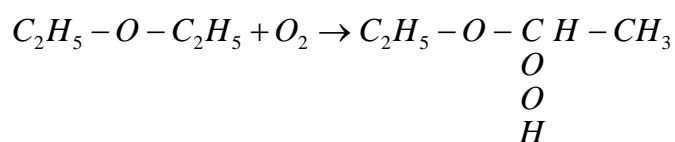


Figure 4. (a) Morphology of a-NFAs after annealing in air at 350 °C for 1 h. (b) XRD patterns of a-NFAs after different annealing treatments. (c) FTIR spectra of a-NFAs after testing at 175 °C and after annealing at 275 and 350 °C for 1 h in air. (d) Response of sensors to DEE (R_g/R_a) or ethanol and isopropanol (R_a/R_g) at 175 °C after they were annealed for 1 h in air at 275 °C (top) and 350 °C (bottom).

Based on the above results, the excellent response of the a-NFAs toward DEE can be understood as follows. The room-temperature synthesis leads to amorphous NFAs with numerous defects and C=O groups on their surface. The outstanding performance of such NFAs can be attributed to three main factors. First, the unique open trumpet-shaped structure of the NFAs (well-seen in Figures 2a and 4a) allows for a quick infusion and adsorption of DEE, thus improving the response speed efficiently. Second, the CBD-prepared amorphous CdO NFAs possess a large number of defects that may contribute to the observed high

response to DEE. Annealing at 275 °C is believed to reduce their density, promoting crystallization of the material but still preserving its surface C=O groups (Figures 4 b,c). Correspondingly, the response to DEE decreases from 3.5 to 2.8, permitting to assume some effect of defects in the as-prepared material on its high gas-sensing response. Third, the abundant C=O groups on their surface can absorb DEE exclusively via the intermolecular forces²¹, thus giving rise to the observed extraordinary selectivity to DEE. While, DEE molecules are easily oxidized to diethyl ether peroxide at working temperature through the following reaction²⁸:



The formed diethyl ether peroxide molecules then attract electrons from the a-NFAs, thus leading to an increase in electrical resistance of the latter flakes, which is well seen as a gas-sensing response in Figure 3b. After high-temperature annealing (350 °C), the surface C=O groups are mainly eliminated (see Figure 4c), and as a result the CdO NFAs do not response to DEE any more. Therefore, we conclude that the observed quick response, high response, and excellent selectivity of the CdO NFAs toward DEE arise, respectively, from the open trumpet-shaped morphology, defect-rich amorphous nature and surface C=O groups of the material.

4. Conclusions

We developed a low-cost process to prepare arrays of amorphous CdO nanoflakes on interdigitated electrodes at room temperature and through a simple chemical bath deposition approach. The as-prepared CdO nanoflake arrays exhibited a quick response (4.5 s), low

detection limit (5 ppm) and superior selectivity (3.8) to diethyl ether, which are the best values reported thus far. The open trumpet-shaped morphology, amorphous structure rich in defects and surface C=O groups are concluded to be responsible for the quick response, high response and excellent selectivity of the material to diethyl ether. This study demonstrates that arrays of amorphous nanoflakes with proper surface groups on their surface are good candidates for gas sensing applications.

Conflict of Interest: The authors declare no competing financial interest.

Acknowledgment

This work was supported by the National Basic Research Program of China (2014CB931703), and the Natural Science Foundation of China (Nos. 51471115 and 51171127). S.A.K. acknowledges support from the Seventh Framework Programme (FP7-PEOPLE-2012-IIF, project no. 330516).

Electronic Supplementary Information available: XPS spectra, EELS spectrum, response of sensor with a-NFAs repeatedly exposed to DEE with concentration of 200 ppm, morphology and XRD patterns of a-NFAs before test and after gas-sensing test for 12 h, response of sensor annealed at 275 °C to 200 ppm of isopropanol, ethanol and DEE, response of sensor annealed at 350 °C to 200 ppm of isopropanol and ethanol. See DOI: .

References

- (1) J.F. Chang, H.H. Kuo, I.C. Leu, and M.H. Hon, The effects of thickness and operation temperature on ZnO: Al thin film CO gas sensor. *Sens. Actuators, B* **2002**, *84*, 258-264.
- (2) M. Hallman, R. Spragg, J.H. Harrell, K.M. Moser, and L. Gluck, Evidence of lung surfactant abnormality in respiratory failure. Study of bronchoalveolar lavage phospholipids, surface activity, phospholipase activity, and plasma myoinositol. *J. Clin. Invest.* **1982**, *70*, 673.
- (3) X. Fu, J. Liu, T. Han, X. Zhang, F. Meng, and J. Liu, A three-dimensional hierarchical CdO

- nanostructure: Preparation and its improved gas-diffusing performance in gas sensor. *Sens. Actuators, B* **2013**, *184*, 260-267.
- (4) W. Sha, P. Gu, B. Zhang, and C. Zheng, A cataluminescence sensor system for diethyl ether based on CdO nanostructure. *Meas. Sci. Technol.* **2014**, *25*, 085102.
 - (5) X. Yu, C. Xie, L. Yang, and S. Zhang, Highly photoactive sensor based on NiO modified TiO₂ porous film for diethyl ether. *Sens. Actuators, B* **2014**, *195*, 439-445.
 - (6) P. Slobodian, P. Riha, A. Lengalova, P. Svoboda, and P. Saha, Multi-wall carbon nanotube networks as potential resistive gas sensors for organic vapor detection. *Carbon* **2011**, *49*, 2499-2507.
 - (7) Y. Liu, Y. Jiao, Z. Zhang, F. Qu, A. Umar, and X. Wu, Hierarchical SnO₂ nanostructures made of intermingled ultrathin nanosheets for environmental remediation, smart gas sensor, and supercapacitor applications. *ACS Appl. Mater. Interfaces*, **2014**, *6*, 2174-2184.
 - (8) Y. Shi, K. Saito, H. Ishikuro, and T. Hiramoto, Effects of traps on charge storage characteristics in metal-oxide-semiconductor memory structures based on silicon nanocrystals. *J. Appl. Phys.* **1998**, *84*, 2358-2360.
 - (9) J.K. Kim, H.J. Cheong, Y. Kim, J.Y. Yi, H.J. Bark, S.H. Bang, and J.H. Cho, Rapid-thermal-annealing effect on lateral charge loss in metal-oxide-semiconductor capacitors with Ge nanocrystals. *Appl. Phys. Lett.* **2003**, *82*, 2527-2529.
 - (10) J.H. Park, S. Kim, and A.J. Bard, Novel carbon-doped TiO₂ nanotube arrays with high aspect ratios for efficient solar water splitting. *Nano Lett.* **2006**, *6*, 24-28.
 - (11) A. Rydosz, Amorphous and nanocrystalline magnetron sputtered CuO thin films deposited on low temperature cofired ceramics substrates for gas sensor applications. *IEEE Sens. J.* **2014**, *14*, 1600-1607.
 - (12) L. Wang, P. Gao, D. Bao, Y. Wang, Y. Chen, C. Chang, G. Li, and P. Yang, Synthesis of crystalline/amorphous core/shell MoO₃ composites through a controlled dehydration route and their enhanced ethanol sensing properties. *Cryst. Growth Des.* **2014**, *14*, 569-575.
 - (13) B.M. Rao and S.C. Roy, Solvothermal processing of amorphous TiO₂ nanotube arrays: achieving crystallinity at a lower thermal budget. *J. Phys. Chem. C.* **2013**, *118*, 1198-1205.
 - (14) H.F. Lu, F. Li, G. Liu, Z.G. Chen, D.W. Wang, H.T. Fang, G.Q. Lu, Z.H. Jiang, and H.M. Cheng, Amorphous TiO₂ nanotube arrays for low-temperature oxygen sensors. *Nanotechnology* **2008**, *19*, 405504.

- (15) N. Asakuma, H. Hirashima, H. Imai, T. Fukui, and M. Toki, Crystallization and reduction of sol-gel-derived zinc oxide films by irradiation with ultraviolet lamp. *J. Sol-Gel Sci. Technol.* **2003**, *26*, 181-184.
- (16) Y.S. Jung, J.Y. Seo, D.W. Lee, and D.Y. Jeon, Influence of DC magnetron sputtering parameters on the properties of amorphous indium zinc oxide thin film. *Thin Solid Films* **2003**, *445*, 63-71.
- (17) Y. Yoshino, T. Makino, Y. Katayama, and T. Hata, Optimization of zinc oxide thin film for surface acoustic wave filters by radio frequency sputtering. *Vacuum* **2000**, *59*, 538-545.
- (18) T. Hitosugi, A. Ueda, S. Nakao, N. Yamada, Y. Furubayashi, Y. Hirose, T. Shimada, and T. Hasegawa, Fabrication of highly conductive $Ti_{1-x}Nb_xO_2$ polycrystalline films on glass substrates via crystallization of amorphous phase grown by pulsed laser deposition. *Appl. Phys. Lett.* **2007**, *90*, 212106.
- (19) D.S. Dhawale, A.M. More, S.S. Latthe, K.Y. Rajpure, and C.D. Lokhande, Room temperature synthesis and characterization of CdO nanowires by chemical bath deposition (CBD) method. *Appl. Surf. Sci.* **2008**, *254*, 3269-3273.
- (20) H. Yin, Y. Wada, T. Kitamura, S. Kambe, S. Murasawa, H. Mori, T. Sakata, and S. Yanagida, Hydrothermal synthesis of nanosized anatase and rutile TiO_2 using amorphous phase TiO_2 . *J. Mater. Chem.* **2001**, *11*, 1694-1703.
- (21) Y. Peng, Z. Meng, C. Zhong, J. Lu, Z. Yang, and Y. Qian, Tube-and ball-like amorphous MoS_2 prepared by a solvothermal method. *Mater. Chem. Phys.* **2002**, *73*, 327-329.
- (22) T. Kavinkumar, D. Sastikumar, and S. Manivannan, Effect of functional groups on dielectric, optical gas sensing properties of graphene oxide and reduced graphene oxide at room temperature. *RSC Adv.* **2015**, *5*, 10816-10825.
- (23) N.A. Travlou, M. Seredych, E. Rodríguez-Castellón, and T. Bandoz, Activated carbon-based gas sensors: effects of surface features on the sensing mechanism. *J. Mater. Chem. A* **2015**, *3*, 3821-3831.
- (24) A.F. Carley, M.W. Roberts, and A.K. Santra, Interaction of oxygen and carbon monoxide with CsAu surfaces. *J. Phys. Chem. B* **1997**, *101*, 9978-9983.
- (25) U. Jain, J. Narang, K. Rani, and N. Chauhan, Synthesis of cadmium oxide and carbon nanotube based nanocomposites and their use as a sensing interface for xanthine detection. *RSC Adv.* **2015**, *5*, 29675-29683.

- (26) P. Thomas, and K.E. Abraham, Excitation wavelength dependent visible photoluminescence of CdO nanomorphotypes. *J. Luminesc.* **2015**, *158*, 422-427.
- (27) J. Karimi Andeani, and S. Mohsenzadeh, Phytosynthesis of cadmium oxide nanoparticles from *Achillea wilhelmsii* flowers. *J. Chem.* **2013**, *2013*, 147613.
- (28) A. Rieche, and R. Meister, Modellversuche zur Autoxydation der Äther. *Angew. Chem.* **1936**, *49*, 101-103.